Environmental Science & Technology

Article

pubs.acs.org/est

Solubility of Iron from Combustion Source Particles in Acidic Media Linked to Iron Speciation

Hongbo Fu,*[,†] Jun Lin,[‡] Guangfeng Shang,[†] Wenbo Dong,[†] Vichi H. Grassian,[§] Gregory R. Carmichael,[§] Yan Li,[‡] and Jianmin Chen*[,†]

[†]Department of Environmental Science and Engineering, Fudan University, Shanghai 200433, China

[‡]Key Laboratory of Nuclear Analysis Techniques, Shanghai Institute of Applied Physics, Chinese Academy of Sciences, Shanghai 201800, China

[§]Center for Global and Regional Environmental Research, Iowa City, Iowa, United States

Supporting Information

ABSTRACT: In this study, iron solubility from six combustion source particles was investigated in acidic media. For comparison, a Chinese loess (CL) dust was also included. The solubility experiments confirmed that iron solubility was highly variable and dependent on particle sources. Under dark and light conditions, the combustion source particles dissolved faster and to a greater extent relative to CL. Oil fly ash (FA) yielded the highest soluble iron as compared to the other samples. Total iron solubility fractions measured in the dark after 12 h ranged between 2.9 and 74.1% of the initial iron content for the combustion-derived particles (Oil FA > biomass burning particles (BP) > coal FA). Ferrous iron represented the dominant soluble form of Fe in the suspensions of straw BP and corn BP, while total dissolved Fe presented mainly as ferric iron in the cases of oil FA, coal FA, and CL. Mössbauer measurements and TEM analysis revealed that Fe in oil FA was commonly presented as nanosized Fe_3O_4 aggregates and Fe/S-rich particles. Highly labile source of Fe in corn BP could be originated from amorphous Fe form mixed internally with K-rich particles. However, Fe in coal FA was dominated by the more insoluble forms of both Fe-bearing aluminosilicate glass and Fe oxides. The data presented herein showed that iron speciation varies by source and is an important factor controlling iron solubility from these anthropogenic emissions in acidic solutions, suggesting that the variability of iron solubility from combustion-derived particles is related to the inherent character and origin of the aerosols themselves. Such information can be useful in improving our understanding on iron solubility from combustion aerosols when they undergo acidic processing during atmospheric transport.

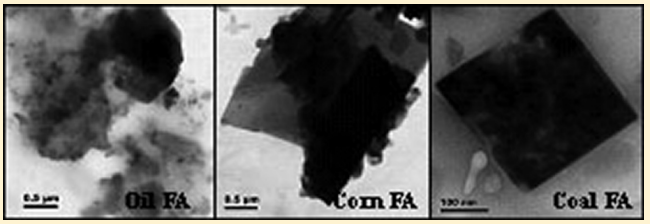

1. INTRODUCTION

Iron is an important micronutrient, and its availability is critical in regulating primary productivity over the ocean. It has been suggested that 30% of the oceans are comprised of high-nutrient low-chlorophyll (HNLC) regions where phytoplankton primary productivity is limited by the amount of bioavailable iron.[1−6] As a result, the supply of bioavailable Fe from atmospheric deposition can modulate CO_2 sequestration and thus influence the global carbon cycle and climate.[2−5]

Desert dust iron is estimated to represent approximately 95% of the globally averaged atmospheric budget, with the remaining fraction attributed to anthropogenic emissions, including industry, fossil fuel, biofuels, and biomass burning.[3] Many previous studies have assumed that mineral aerosols from arid and semi-arid continental regions are a major source of Fe to the remote ocean.[7−15] Measuring the soluble Fe fraction along with understanding processes that control Fe solubility is important since soluble Fe is associated with the amount of bioavailable Fe.[1,5] Several studies suggest that most of the soluble iron is linked to chemical processing of dust during long-range atmospheric transport, because soluble iron in soils is on average less than 0.1%, whereas measurements of iron in aerosols suggest a much higher solubility (up to 80%).[2−6] This "chemical processing" is generally thought to involve the reduction of Fe(III) to Fe(II), mediated by the presence of acidic species,[7−9] sunlight,[10−12] and cloudwater condensation and evaporation.[13−15] Especially, some researchers emphasized the importance of photooxidation in the presence of acids in cloudwater.[16,17] At present, however, there is no compelling field evidence that links enhanced aerosol iron solubility to atmospheric chemical processing. Furthermore, model predictions of aerosol iron solubility as a function of atmospheric chemical processing show the simulated iron solubility (1−2%) is much lower than that derived from field measurements (10−

Received: June 26, 2012
Revised: September 3, 2012
Accepted: September 10, 2012
Published: September 10, 2012

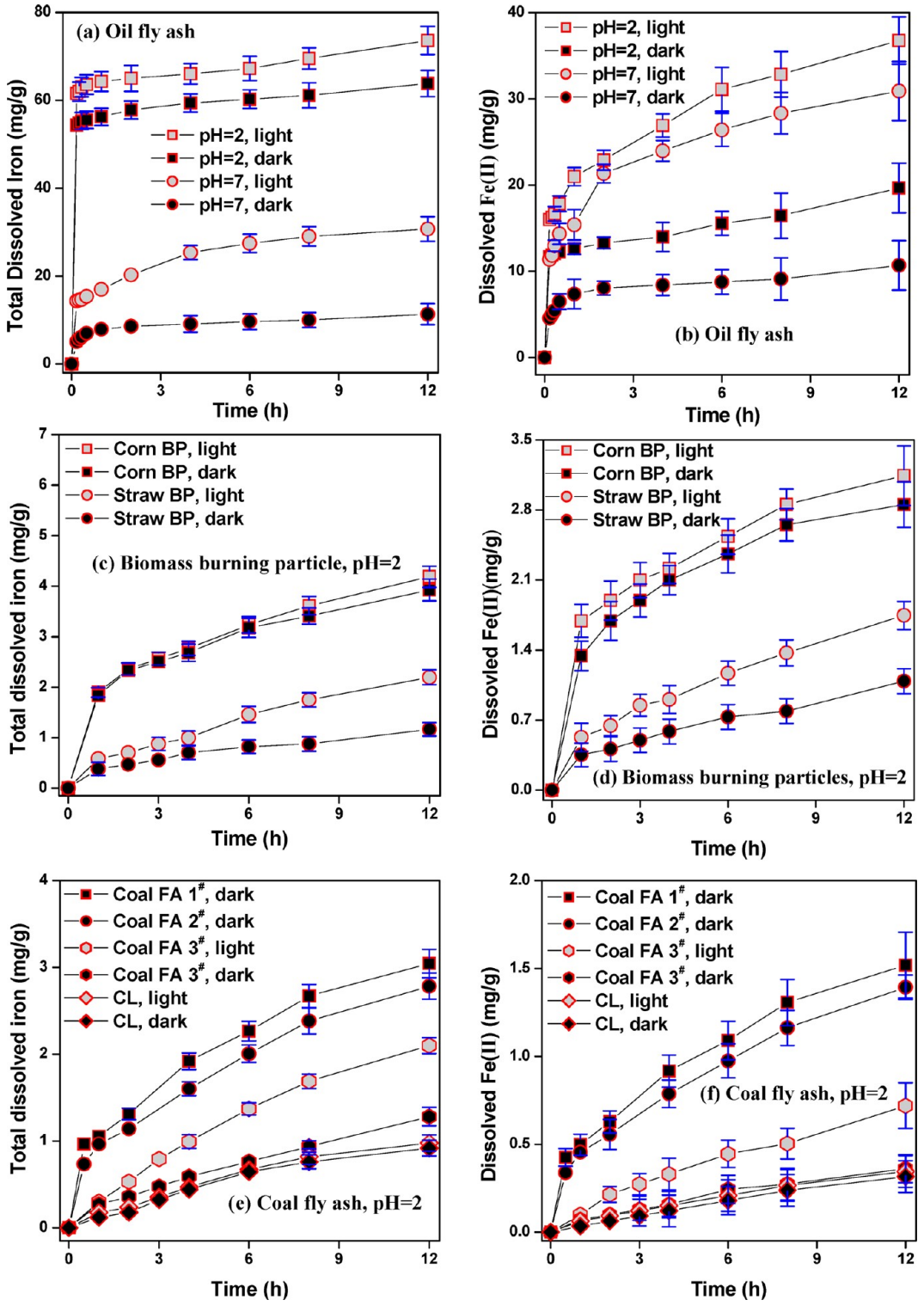

Figure 1. Comparison of Fe solubility from combustion-derived particles and CL in the dark or under the irradiation as a function of time in HCl suspensions. Calculated solubilities are shown for total dissolved iron and dissolved Fe(II). Reactors contained a solids loading of 1.5 g/L. When present, uncertainties represent one standard deviation from triplicate experiments. mg/g in *y*-axis labels represents mg of soluble Fe per gram of the solid particle.

40%), suggesting additional processes and/or sources may contribute to Fe dissolution.[3]

Recent attention has focused on anthropogenic sources.[3,18−30] Several lines of evidence suggest combustion-derived aerosols as a significant source of soluble aerosol Fe, in contrast to its supply from mineral aerosols.[18−29] Based on an observed high correlation between soluble iron and black carbon on a yearly average, Chuang et al. concluded that soluble iron comes predominately from combustion sources.[18] The work of Guieu et al. revealed that biomass burning may be an important input of iron to the Mediterranean Sea relative to Saharan dust input.[19] Sholkovitz et al. suggested that anthropogenic

combustion emissions contribute approximately 85% of the soluble iron to the surface ocean near Ireland, implying that human activities have profoundly affected the iron budget of the North Atlantic region.[20] In fact, this concept has been further strengthened by a modeling study by Luo et al., which suggested that the best match to available data included substantially higher solubilities of iron in combustion aerosols than in dust (4% versus 0.4%).[21]

Processes that control Fe solubility in combustion aerosols still remain enigmatic. Several recent studies have also emphasized that aerosol mineralogy, especially iron chemical form in aerosols, could be a critical factor for Fe mobilizing.[28,31−34] Journet et al. supposed that iron solubility can be linked to the chemical specificity of the bonds in which iron is coordinated in the different minerals.[31] Cwiertny et al. proposed that the iron in the form of Fe(II) in dust aerosol is a highly labile source of iron under acidic conditions.[7] More recently, Schroth et al. have documented very high solubility of iron in oil fly ashes, in which iron speciation is mainly as ferric salts.[23] Although iron solubility in combustion aerosols could be heavily influenced by iron speciation, no such relationship has yet been clearly established, largely owing to a lack of direct laboratory measurements of iron speciation.

In this paper, we present iron solubility measurements in acidic solutions, since a deliquescent liquid layer with pH less than 2 can occur on particle surfaces in the atmosphere.[7] Coal FA, heavy oil FA, and biomass BP were selected because they are representative of important types of combustion source particles. To deduce the relationship between iron solubility and its speciation, Mössbauer spectroscopy and single-particle TEM analysis were employed to characterize these samples. CL was also included for comparison, to explore the contribution of bioavailable iron from combustion emissions relative to mineral dust. Our goal is to provide a more comprehensive understanding of Fe solubility from combustion aerosols in aqueous environments at low pH associated with atmospheric aerosol under certain atmospheric conditions.

2. EXPERIMENTAL SECTION

Sampling. Coal fly ash samples (Coal FA 1#−3#) were collected from the hoppers of electrostatic precipitators of three pulverized coal-fired power plants. Both coal FA 1# and coal FA 2# were collected from the plants fueled by bituminous coals from Datong city and Taiyuan city, Shanxi province, respectively. Coal FA 3# was collected from the plant fueled by lignite from Hailaer city, The Inner Mongolia Autonomous Region. The burning of harder, older bituminous coal typically produces Class F fly ash, whereas the burning of lignite produces Class C fly ash. Oil FA was collected from a heavy oil-fired boiler in Shenyang city, Liaoning province. Corn and rice are the most important crops, and they have a wide distribution in China. Corn stalk and rice straw were gained from Shangdong province and Shanghai city, respectively. They were burned in a homemade stove, and subsequently residual ash particles were collected (corn BP and straw BP). CL was collected from Yulin city, Shanxi province, which was friendly supplied by Institute of Earth Environment, Chinese Academy of Sciences. With the exception of CL, all of the samples were dry-sieved to <50 μm. The samples were stored in sealed vials to minimize exposure to ambient air and preserve them for further analysis.

Fe Dissolution Measurements. The experiments were carried out in a custom-made glass reactor using the collected particles. At each sampling event, enough sample volume was taken to allow for analysis of dissolved iron species colorimetrically with 1,10-phenanthroline. This colorimetric measurement has been described previously in detail.[10] Further details were provided in the Supporting Information.

Methods and Analysis. Total iron content of these samples was determined from the analysis of acid-digested samples via inductively coupled plasma atomic emission spectroscopy (ICP−AES). Mössbauer measurements were performed in transmission geometry with a constant acceleration. ^{57}Co (Pd) was used as the Mössbauer source, and a 1 mm thick Na(TI) scintillator coupled to a EMI9750B photoelectric multiplier was used as the detector. The TEM grid samples were examined with a JEOL-2100F field emission high-resolution TEM (FE-HRTEM) equipped with an Oxford energy-dispersive X-ray spectrometer (EDS). The samples were prepared on the basis of the previous work.[35,36] Additional details of the methods were provided in the Supporting Information.

3. RESULTS AND DISCUSSION

Iron Solubility. Results comparing the dissolution of each sample are shown in Figure 1, which presents solubility data for total dissolved Fe and dissolved Fe(II) as a function of time. The solubility experiments confirmed that Fe solubility was highly variable and dependent on FA source. Under dark and light conditions, it could be clearly seen that the combustion source particles dissolved faster and to a greater extent relative to CL. Oil FA yielded the highest solubility of total dissolved Fe as compared to the other particles. The amount of soluble Fe from oil FA was higher by 2 orders of magnitude than that from CL. In pH 2 suspensions, total dissolved Fe and the dissolved Fe(II) from oil FA reached 63.8 mg/g and 19.7 mg/g in the dark after 12 h, whereas total dissolved Fe and the dissolved Fe(II) from CL only reached 0.9 mg/g and 0.3 mg/g, respectively. Furthermore, the initial period of Fe mobilized from the oil FA particles was extremely fast with total dissolved Fe reaching 54.4 mg/g within 5 min. After a sharp increase, total dissolved iron increase gradually toward a plateau. Such iron dissolution kinetic suggests that oil FA particles could contain the iron species that dissociate immediately upon contact with water. Comparing two biomass-burning samples, corn BP shows much higher Fe dissolution than that of straw BP. The amount of Fe released from corn BP reached 3.9 mg/g in the dark after 12 h, which were roughly 4.3 times of the Fe amount leased from CL. In the case of coal FA, both coal FA 1# and coal FA 2# released higher concentration of dissolved Fe as compared to CL. After 12 h, 3.0 mg/g and 2.8 mg/g of total dissolved Fe were released from coal FA 1# and coal FA 2#, which were 3.3 and 3.1 times of the Fe amount mobilized from CL, respectively. However, total dissolved iron concentrations in straw BP and coal FA 3# were extremely low. Only 1.3 mg/g and 1.2 mg/g of total dissolved Fe were released from coal FA 3# and straw BP after 12 h in the dark, both of which were comparable with the amount released from CL. The trends in Fe solubility observed in three of the coal FA samples could be related to differences in coal types. In all the cases, the dissolved Fe(II) showed the similar trend with total dissolved Fe mobilized from the samples.

Specifically, ferrous iron represented the dominant soluble form of the Fe in the pH 2 suspensions of the biomass burning particles, while total dissolved Fe present mainly as ferric iron in the case of oil FA, coal FA, and CL. The relative proportion

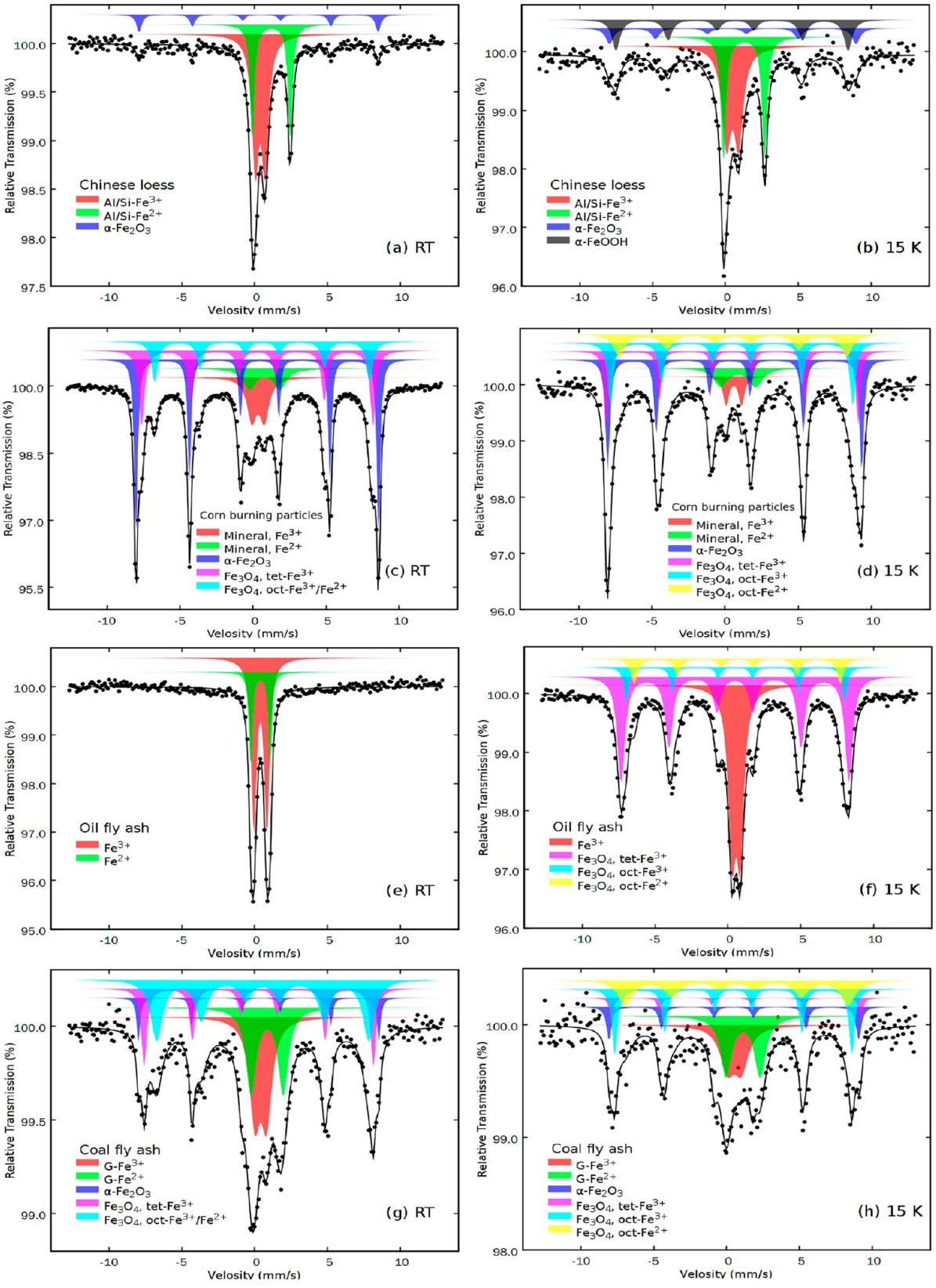

Figure 2. Mössbauer spectroscopy measured at RT and 15 K for CL and the combustion-derived particles. CL at RT (a) and 15 K (b), Corn BP at RT (c) and 15 K (d), Oil FA at RT (e) and 15 K (f), and Coal FA 1# at RT (g) and 15 K (h), respectively. Experimental data were fitted by a least-squares fitting-program. The normalized chi-squares were in the range of 1−4, and the fitting error for the parameter was as follows: IS, 0.02 mm/s; QS, 0.02 mm/s; H_f, 0.1 T, respectively. The relative content of iron could be calculated according to the area of subspectra as shown in Table S1. Prominent spectral features associated with different iron species were labeled.

of dissolved Fe(II) reached 95% and 81% in the suspensions of corn BP and straw BP in the dark after 12 h. However, only 28% and 33% of total dissolved Fe were presented as ferrous iron in the case of oil FA and CL. As for three coal FA samples, the relative proportion of dissolved Fe(II) was approximately 35% on average (Figure S1). This behavior suggests that differences exist in the relative rate and extent of dissolution of the Fe(II)- and Fe(III)-containing solid phases present in combustion source particles. Ferrous iron representing the dominant soluble form in the cases of biomass burning particles supported the recent field-measurements. Trapp et al. revealed that Southern Africa outflow sourced from biomass burning contained large soluble iron fractions with high Fe(II)/Fe(III) ratios.[34] Based on a single-particle analysis, Takahama et al. proposed that organic matrix in biomass burning particles could prevent Fe(II) from subsequent oxidation in the atmosphere.[37]

Total dissolved Fe was greater in irradiated suspensions than dark suspensions in most cases. Oil FA yielded the highest solubility of total dissolved Fe species when exposed to the irradiation, and the amount of total dissolved iron increased by 15% at pH = 2 compared to the dark reaction. Light also promoted greatly the formation of dissolved Fe(II) in all the cases. In particular, a significant enhancement of dissolved Fe(II) was observed in the oil FA suspensions. Upon exposure of the oil FA suspension to light for 12 h, the concentration of dissolved Fe(II) increased by 87% at pH = 2 compared to the dark reaction. For straw BP and coal FA 3#, the presence of light promoted apparently Fe solubility; whereas no discernible changes in the concentration of total dissolved Fe were observed for the irradiated suspension of CL.

The experiments were also conducted in aqueous solutions at pH 7.0. For the oil FA particle, the amount of total dissolved Fe reached 11.3 mg/g. Upon exposure of the oil FA suspension to light, the concentration of total dissolved Fe increased greatly by 1.7 times as compared to the dark reaction. Notably, pH of the solution had a stronger effect than irradiation for total dissolved iron in the suspensions of oil FA; whereas irradiation had a stronger effect than pH of the solution for dissolved Fe(II).

Mössbauer Spectroscopic Analysis. Mössbauer spectra collected at RT and 15 K were used to identify the oxidation states of iron within each sample, as shown in Figure 2. The corresponding hyperfine parameters estimated from the best-fitted spectra are presented in Table S1.

In the case of CL, the spectra at RT could be successfully fitted using two central quadrupole doublets and one magnetic hyperfine split (MHS) sextets. The central doublet with isomer shift (IS) = 0.38 mm s^{-1} is typical for high-spin Fe^{3+} in octahedral symmetry, while the other one with IS = 1.14 mm s^{-1} is characteristic of high-spin Fe^{2+}.[38−40] Both of the doublets do not magnetically order to a sextet at our lowest achievable analytical temperature of 15 K, consistent with the presence of Fe-substituted aluminosilicates in the sample.[7] Estimates of the quadrupole splitting (QS) 0.67 mm/s for Fe^{3+} and 2.61 mm/s for Fe^{2+} are also in agreement with those reported for Fe forms in aluminosilicate minerals.[38,41] As for the MHS sextet, the IS, QS, and H_f are 0.38 mm/s, −0.21 mm/s, and 51.0 T at RT and 0.43 mm/s, 0.40 mm/s, and 52.8 T at 15 K, respectively. In terms of these obtained Mössbauer parameters, it could be ascribed to α-Fe_2O_3.[41] The QS value from negative to positive change is originated from Morin transition of α-Fe_2O_3 (T_m = 263 K), which is due to the sudden change of spin direction.[41] Upon cooling, the most noticeable feature that emerges is the strengthening of the magnetically ordered components at the expense of the doublets. This is due to the progressive blocking in superparamagnetic grains as the temperature is lowered.[41] The outer component with H_f = 52.8 is clearly weakly ferromagnetic α-Fe_2O_3 in which the Morin transition has been suppressed below 12 K due to foreign element substitution and/or fine grain sizes.[41] At 15 K, a new sextet with IS = 0.57 mm/s and H_f = 49.8 mm/s appears besides the components appearing at RT is possibly α-FeOOH.[40,42] Two central quadrupole doublets at the 15 K spectrum represent 65% of the whole area, suggesting that Fe-substituted aluminosilicates in CL is the main Fe species. Both α-Fe_2O_3 and α-FeOOH share the remaining part.

The spectra of corn BP at RT show two QS doublet components and three MHS sextets. The doublets in the central part of the spectra with IS = 0.34 mm/s and QS = 0.86 mm/s arise from the presence of high spin Fe^{3+} species, whereas those with IS = 0.79 mm/s and QS = 2.08 mm/s are attributed to high spin Fe^{2+} species.[39] Three sextets with corresponding H_f of 51.6, 49.3, and 45.7 for S_1, S_2, and S_3 in the spectra are due to Fe in oxidic, which are the main components in the spectrum of the sample. The sextet with H_f = 51.6 is typical for α-Fe_2O_3, while the other two with H_f = 49.3 and 45.7 mm s^{-1} are characteristic of Fe_3O_4.[39] In Fe_3O_4, the iron is situated in the two crystallographically inequivalent tetrahedral A and octahedral B sites.[38] The spectrum of Fe_3O_4 at RT is composed of only two sextets (S_2 and S_3). S_2 corresponds to Fe^{3+} cations on a tetrahedral site, while S_3 corresponds to Fe^{2+} and Fe^{3+} cations on an octahedral site.[42] When the spectra was taken above the Verwey transition temperature (T_V = 120 K), a fast electron-transfer between Fe^{2+} and Fe^{3+} in octahedral structure occurs, resulting in a sextet of S_3. Below T_V (T = 15 K), the relaxation time becomes longer. As a consequence, Fe^{2+} and Fe^{3+} in octahedral sites can be differentiated from two independent sextets of S_3 and S_4 at the spectrum collected at 15 K.[42] The peak areas of S_2−S_4 totally share 50% of the whole area. Therefore, we may assume that the main composition of the iron-containing particles is Fe_3O_4, along with lesser fractions of the α-Fe_2O_3 particles. The Mössbauer spectrometer used herein has not detected any Fe signal from straw BP, which could be due to the low iron content in this sample.

Figure 2e and f show Mössbauer spectra and their fitted results for oil FA. In the spectrum at RT, there are only two central quadrupole doublets besides a small contribution from the small background. Upon cooling, there are two components, one consists of a doublet and another consists of three sextets, while the central quadrupole doublets appearing at RT disappear completely. This result indicates that the iron particles in the aerosols are very small, showing a superparamagnetic behavior at RT and ferromagnetic mostly at 15 K. Such behavior of the particles shown in a Mössbauer spectrum typically belongs to nanosized ferromagnetic or antiferromagnetic particles due to magnetic spin relaxation.[38] When the particle is small enough, the magnetic vectors of particles will flip to various directions due to thermal disturbance and exhibit superparamagnetism effect. The characteristic relaxation life can be expressed as follows: $\tau = 1/af \exp(KV/k_BT)$, where f is the frequency of Larmor precession, a is the geometric factor, K is the anisotropy energy density, V is the volume, and k_B is Boltzmann's constant.[38,43] By lowering the temperature, the characteristic relaxation time τ will be "slowing down", which will eliminate superparamagnetic of ultrafine particles.[43] The main doublet of the component,

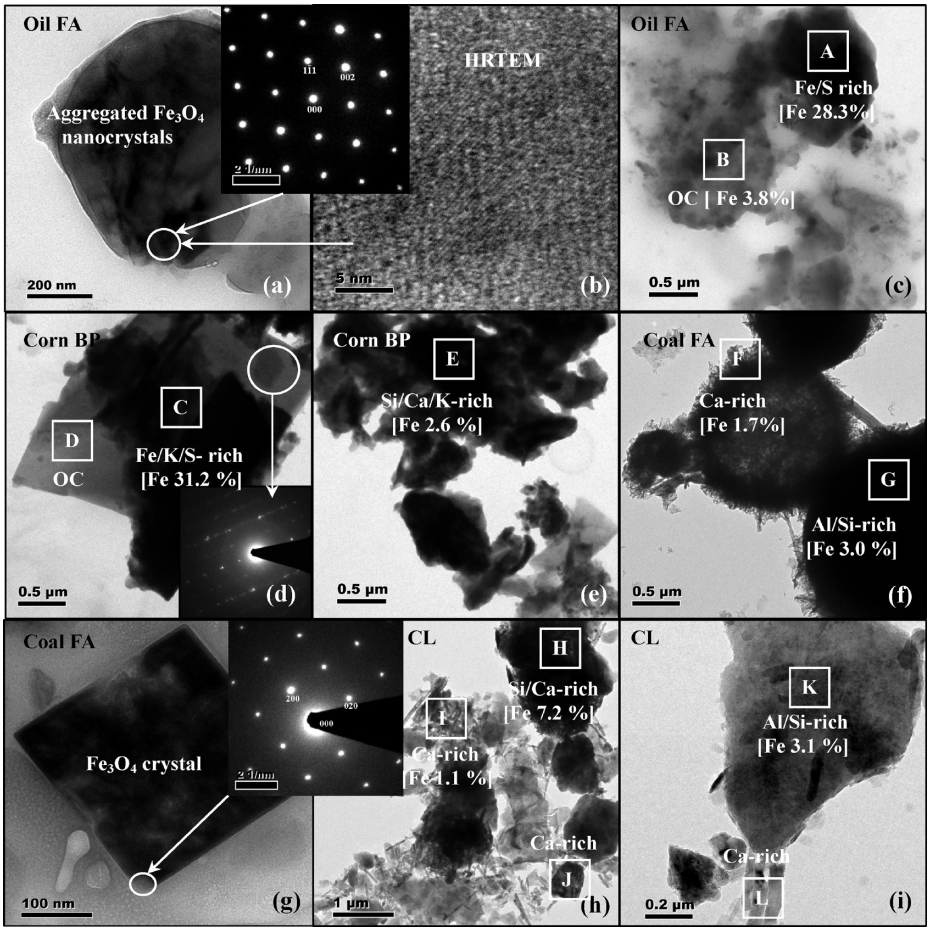

Figure 3. Various types of Fe-bearing particles in the combustion source particles and CL identified using TEM. The compositions were determined using energy dispersive X-ray spectrometry. The letter boxes denote the positions where EDS spectra were taken. The dotted white circles indicate the area of the electron beam for high-resolution TEM or SAED patterns. Elements of the detected parts of individual particles are in parentheses. Square brackets indicate mass percent of iron. (**a**) The aggregated Fe_3O_4 nanocrystals are covered by a carbonaceous matrix, based on their compositions and crystal structures from the SAED measurement. The SAED pattern in the inset displays the [110] zone axis of the crystal. This morphology is abundant in *oil FA*; (**b**) the high-resolution image gained from the dotted white circle in part a shows the lattice fringe of Fe_3O_4 nanocrystal; (**c**) the Fe/S-rich particles in *oil FA*. The areas with high Fe amount appear darker than the ones containing low Fe amount; (**d**) Fe/K/S-rich particle is attached to the flatlike OC particle in *corn BP*. As a result of diffraction contrast, the Fe-rich particle appears darker than the material of their host particle; (**e**) Overview showing agglomerate of Si/Ca/K-rich particles with Fe inclusions in *corn BP*; (**f**) the aggregated Fe-bearing aluminosilicate spheres covered by Ca-rich coatings in *coal FA*; (**g**) An octahedral Fe-rich crystal in *coal FA*. The SAED pattern is indexed as Fe_3O_4 that has a spinel crystalline structure. The SAED pattern gained from the tip of the crystal displays the [002] zone axis of the crystal; (**h**) the aggregated Fe-bearing aluminosilicate and Ca-rich particles in *CL*; (**i**) the irregularly shaped aluminosilicate clays with Fe inclusion in CL. Bar-shaped particles are Ca-rich.

with IS = 0.56 mm/s, QS = 0.56 mm/s, may be due to the high-spin Fe^{3+} state in $KFe_3(SO_4)_2(OH)_6$ and/or $Fe_3(PO_4)_2$.[38] On the basis of the NEXAFS analysis, Schroth et al. ascribed the main Fe species in oil FA to Fe sulfates.[23] As discussed above, three sextet with H_f from 43.8 to 48.8 T and IS from 0.49 to 0.53 mm/s could be originated from superfine Fe_3O_4 nanoparticles.[39]

The spectra of three coal FAs are similar. At RT, all of three samples show two central quadrupole doublets and three MHS sextets. One doublet, with IS = 0.41−0.42 mm/s and QS = 0.80−0.94 mm/s, may be ascribed to Fe^{3+}-glass.[44] The other doublet, characterized by IS = 0.81−0.92 mm/s and QS = 2.21−2.26 mm/s, is typical for Fe^{2+}-glass.[44] S_1 with H_f = 50.9−51.3 mm/s is typical for α-Fe_2O_3.[27] S_2 and S_3, which changed into three sextets of S_2, S_3, and S_4 at the 15 K spectra, were considered to be due to the Verway transition of Fe_3O_4.[39] The occurrence of iron oxides in coal FA is due to the transformation of Fe-sulfides and sulfates.[45] From the peak areas of the doublets for various samples, it can be found that Fe_3O_4 is an important Fe species in coal FA, which is in good agreement with the previous reports.[45]

Typical TEM Aanlysis. The Fe-bearing particles in oil FA were categorized into two different types based on their morphological and X-ray spectral data (Table *S*2). The first type is of aggregated Fe nanocrystallines with sizes of several dozens of nanometers (Figure 3a). The lattice constant derived from the SAED pattern is very close to that of pure magnetite (the inset of Figure 3a), which is in good agreement with the Mössbauer measurement. The second type is of the amorphous Fe compositions internally mixed with S-rich particles, possibly Fe sulfates (Figure 3c). Fe/S-rich particles were encountered more frequently than Fe in the oxide form and typically incorporate minor amounts of other elements such as Ca, K, V, and Zn.[46]

Potassium-salt particles were the most abundant inorganic constituents in corn BP. They included KCl and K_2SO_4, and

minor K- and Ca-bearing sulfate with variable K ratio. These potassium salts were very beam-sensitive. Most of the KCl particles had euhedral morphologies, and some were rounded (Figure S2a and b). The SAED patterns of KCl and NaCl particles were obtained to confirm their crystallinity. Minor amounts of soot and "tar balls" were also present. Iron in corn BP was found in the form of amorphous Fe compositions internally mixed with the other particles including C, Si, Ca, K, or S elements. Furthermore, Fe-bearing particles generally present irregularly shaped (Figure 3d and e). As a result of diffraction contrast, the Fe-rich particle appeared darker than the material of their host particle (Figure 3d). TEM−EDS revealed that iron is unevenly distributed in corn BP. Among the observed 57 particles, most of grains were entirely free of iron; only four of them exhibited highly varied iron content (2.6%−31.2%), indicating that iron in the plant distribution is not uniform. In the case of straw BP, iron-bearing particles were not identified due to the low iron content.

The characteristic morphologies of coal FA particles were mainly spherical with smaller particles typically attached to larger ones, as demonstrated in the representative TEM image (Figure 3f and Figure S2 h). These spherical particles contained mainly Al and Si components with highly varying K, Ti, Ca, and Fe, which agreed with previous measurements.[27,47,48] The aluminosilicate-bearing ferroxides were often covered by the Ca-rich coating and typical sizes of a few of micronmeters. The spherical shape is due to the molten nature of the material at high temperatures when the particles are formed during coal combustion.[47] Some irregularly shaped particles, mainly Si/Ca- and Si/Ti-rich, were also less encountered. Though much less frequent, Fe_3O_4 crystals were observed as well.

Chinese loess particles were characterized by high fractions and intensities of aluminum and silicon, likely in the form of aluminosilicates, along with other crustal elements including Mn, Ca, K, and Fe. These aluminosilicate particles had the typical sizes larger than 0.5 μm. The particles showed a great deal of variability in combination of three different clusters: aluminosilicate dust, Si-rich dust, and Ca-rich dust (Figure 3h and i). Among the 54 particles observed herein, a majority of particles fall within these three groups of particles with varied Fe content (~9%), consistent with Fe being predominantly substituted into alumionosilicate phase in CL. In contrast to coal FA particles, the mineral particles displayed irregular and rough morphologies due to a mixture of different mineral crystals within a single particle.

Iron Solubility Linked to Iron Species. In order to make relevant comparisons of the iron released from each sample, we defined soluble Fe(II) and total iron solubility as the dissolved concentration measured at 12 h normalized to the total iron content initially present, which was determined from ICP at the present work. The results are shown in Table 1. Fe in oil FA was extremely soluble, releasing 74.1% of total iron content. Fe in corn BP and straw BP were more soluble than Fe sourced in CL, with total solubility reaching 8.9% and 26.4% after 12 h, which are much higher than 4.3% of CL. However, the coal FA samples yielded the lowest solubility fractions. Only 3.9%, 2.9%, and 4.2% of total Fe were mobilized from coal FA 1#, coal FA 2#, and coal FA 3#, respectively.

Several recent studies have recommended that the mineralogy of iron in aerosols is a critical factor for predicting Fe solubility.[23,49] Based on Mössbauer measurements and TEM analysis, iron speciation for the samples in this study was summarized in Table S3. Highly soluble Fe in oil FA could be closely linked to Fe_3O_4 nanoparticles and amorphous Fe/S-rich particles. It has been hypothesized that iron nanoparticles may be more chemically reactive and possibly more bioavailable.[14,50] Furthermore, oil FA could release around 10% of the Fe amount within 5 min at pH 7, suggesting a fraction of Fe in oil FA present as the form that dissociate immediately upon contact with water, such as iron sulfate.[23] Recently, Schroth et al. have documented that almost 70% of iron in oil FA was released in ultrapure Milli-Q solutions, which was much higher than that in this work (11.4%, pH 7). On the basis of the synchrotron-based X-ray absorption spectroscopy, they proposed that Fe in oil FA was mainly presented as ferric sulfate.[23] Although Fe in corn BP and coal FA present mainly crystal Fe_3O_4 from Mössbauer analysis, iron in corn BP were much more soluble as compared to ones in coal FAs. A fraction of Fe in corn BP was internally mixed with K-rich particles, which seemed in the amorphous form. This fraction of iron could be responsible for higher Fe released from corn BP. Coal FA has a crustal-like composition with a great amount of Fe-bearing aluminosilicate glass;[27] therefore, coal FA released the comparable iron fraction with CL. Journet et al. have suggested that the solubility is much higher for the minerals where the Fe is probably found as amorphous form as compared to the Fe in oxides or bound by covalent bonds in the aluminosilicate matrix.[31] Coal FA may still represent a significant source of bioavailable iron due to much higher iron content in coal FA (8.2% of total iron content on average), although Fe in coal FA was more insoluble as compared to one in dust particles, such as CL (3.1% of total iron content).

Table 1. Properties of the Samples and Fe Solubility Fractions (%) Investigated in the Current Study

	surface area (m^2/g)	total iron content (%)	soluble Fe(II) (%)[a]		total Fe solubility (%)[a]	
			light	dark	light	dark
Coal FA 1#	4.8	10.2	-	1.2	-	3.9
Coal FA 2#	5.6	11.9	-	0.8	-	2.9
Coal FA 3#	0.8	3.7	2.7	1.3	8.3	4.2
Oil FA	1.7	9.3	41.8	20.9	85.9	74.1
Corn BP	4.1	3.3	9.7	9.1	12.5	8.9
Straw BP	3.7	0.4	37.0	25.4	41.2	26.4
CL	9.6	3.1	1.6	1.4	4.5	4.3

[a]In order to make relevant comparisons of the iron released from each sample, we define soluble Fe(II) and total iron solubility as the dissolved concentration of each species measured at 12 h normalized to the total iron content initially present in the HCl suspensions at pH 2. The amount of iron initially present was determined from ICP-AES. Specific surface area was gained from N_2-BET. The experiments were repeated for two times.

Atmospheric Implications. Combined evidence from modeling, laboratory, and field observations have suggested that combustion-derived aerosols provide an important source of highly-soluble aerosol Fe.[18−29] However, of the studies available, the combustion source aerosols were usually considered as a generalized classification (such as "anthropogenic emission" or "fossil-fuel combustion") when mentioned as a potential supplier of soluble iron,[3] with no distinction between the combustion sources, i.e. oil vs coal vs biomass. Our results clearly showed that Fe dissolution behavior from different combustion sources in acidic condition

varied greatly. The differences in dissolution behavior are linked to differences in Fe mineralogy and the iron-containing particle sizes within the samples. These results pointed out the oversimplification that arises when treating all combustion particles as having the same degree of Fe acid-mobilization.

Our results also revealed that both oil FA and biomass BP yield much higher Fe solubility fractions than that of CL in acidic solutions, which could be due to the fact that these samples contained highly labile Fe mineralogy, such as Fe sulfate and amorphous form of Fe. Furthermore, a significant contribution of soluble Fe(II) can come from biomass burning, which represents a more bioavailable form of iron. Although Fe in coal FA is relatively insoluble compared to CL, coal FA has a high iron content (around 2−4 times of CL), so that coal FA can release more total dissolved iron compared to CL. On the basis of these results, it can be proposed that combustion source particles could be potential suppliers of bioavailable Fe once they undergo acidic processing during atmospheric transport.

■ ASSOCIATED CONTENT

Supporting Information

Experimental Section, Figures *S*1 and *S*2, and Tables *S*1−*S*3. This material is available free of charge via the Internet at http://pubs.acs.org.

■ AUTHOR INFORMATION

Corresponding Author

*E-mail: fuhb@fudan.edu.cn (H.F.), chenjm@fudan.edu.cn (J.C.).

Notes

The authors declare no competing financial interest.

■ ACKNOWLEDGMENTS

Financial support was provided by National Natural Science Foundation of China (Nos. 40975074, 21177026, 21190053, and 11005144), The Ministry of education of new century talent project (NCET-11-0104), and The Pujiang Talent Program of Shanghai (PJ[2010]00317).

■ REFERENCES

(1) Martin, J. H.; Gordon, R. M.; Fitzwater, S. E. Iron in Antarctic waters. *Nature* **1990**, *345*, 156−158.

(2) Jickells, T. D.; An, Z. S.; Andersen, K. K.; Baker, A. R.; Bergametti, G.; Brooks, N.; Cao, J. J.; Boyd, P. W.; Duce, R. A.; Hunter, K. A.; Kawahata, H.; Kubilay, N.; Roche, J.; Liss, P. S.; Mahowald, N.; Prospero, J. M.; Ridgwell, A. J.; Tegen, I.; Torres, R. Global iron connections between desert dust, ocean biogeochemistry, and climate. *Science* **2005**, *308*, 67−71.

(3) Mahowald, N. M.; Engelstaedter, S.; Luo, C.; Sealy, A.; Artaxo, P.; Benitez-Nelson, C.; Bonnet, S.; Chen, Y.; Chuang, P. Y.; Cohen, D. D.; Dulac, F.; Herut, B.; Johansen, A. M.; Kubilay, N.; Losno, R.; Maenhaut, W.; Paytan, A.; Prospero, J. A.; Shank, L. M.; Siefert, R. L. Atmospheric iron deposition: Global distribution, variability, and human perturbations. *Annu. Rev. Mar. Sci.* **2009**, *1*, 245−278.

(4) Martin, J. H.; Coale, K. H.; Johnson, K. S.; Fitzwater, S. E.; Gordon, R. M.; Tanner, S. J.; Hunter, C. N.; Elrod, V. A.; Nowicki, J. L.; Coley, T. L.; Barber, R. T.; Lindley, S.; Watson, A. J.; Vanscoy, K.; Law, C. S.; Liddicoat, M. I.; Ling, R.; Stanton, T.; Stockel, J.; Collins, C.; Anderson, A.; Bidigare, R.; Ondrusek, M.; Latasa, M.; Millero, F. J.; Lee, K.; Yao, W.; Zhang, J. Z.; Friederich, G.; Sakamoto, C.; Chavez, F.; Buck, K.; Kolber, Z.; Greene, R.; Falkowski, P; Chisholm, S. W.; Hoge, F.; Swift, R.; Yungel, J.; Turner, S.; Nightingale, P.; Hatton, A.; Liss, P.; Tindale, N. W. Testing the iron hypothesis in ecosystems of the equatorial Pacific Ocean. *Nature* **1994**, *371*, 123−129.

(5) Mahowald, N. M.; Baker, A. R.; Bergametti, G.; Brooks, N.; Duce, R. A.; Jickells, T. D.; Kubilay, N.; Prospero, J. M.; Tegen, I. Atmospheric global dust cycle and iron inputs to the ocean. *Global Biogeochem. Cycles* **2005**, *19*, GB4025 DOI: 10.1029/2004GB002402.

(6) Zhuang, G. S.; Yi, Z.; Duce, R. A.; Brown, P. R. Link between iron and sulphur cycles suggested by detection of Fe(II) in remoate marine aerosols. *Nature* **1992**, *355*, 537−539.

(7) Cwiertny, D. M.; Baltrusaitis, J.; Hunter, G. J.; Laskin, A.; Scherer, M. M.; Grassian, V. H. Characterization and acid-mobilization study of iron-containing mineral dust source materials. *J. Geophys. Res.* **2008**, *113*, D05202 DOI: 10.1029/2007JD009332.

(8) Shi, Z.; Bonneville, S.; Krom, M. D.; Carslaw, K. S.; Jickells, T. D.; Baker, A. R.; Benning, L. G. Iron dissolution kinetics of mineral dust at low pH during simulated atmospheric processing. *Atmos. Chem. Phys.* **2011**, *11*, 995−1007.

(9) Solmon, F.; Chuang, P. Y.; Meskhidze, N.; Chen, Y. Acidic processing of mineral dust iron by anthropogenic compounds over the north Pacific Ocean. *J. Geophys. Res.* **2009**, *114*, D02305 DOI: 10.1029/2008JD010417.

(10) Fu, H.; Cwiertny, D. M.; Carmichael, G. R.; Scherer, M. M.; Grassian, V. H. Photoreductive dissolution of Fe-containing mineral dust particles in acidic media. *J. Geophys. Res.* **2010**, *115*, D11304 DOI: 10.1029/2009JD012702.

(11) Zhu, X.; Prospero, J. M.; Savoie, D. L.; Millero, F. J.; Zika, R. G.; Saltzman, E. S. Photoreduction of iron (III) in marine mineral aerosol solutions. *J. Geophys. Res.* **1993**, *98* (D5), 9039−9046.

(12) Key, J. M.; Paulk, N.; Johansen, A. M. Photochemistry of iron in simulated crustal aerosols with dimethyl sulphide oxidation products. *Environ. Sci. Technol.* **2008**, *42*, 133−139.

(13) Shi, Z.; Krom, M. D.; Jickells, T. D.; Bonneville, S.; Carslaw, K. S.; Mihalopoulos, N.; Baker, A. R.; Benning, L. G. Impacts on iron solubility in the mineral dust by processes in the source region and the atmosphere: A review. *Aeolian Res.* **2012**, *5*, 21−42.

(14) Shi, Z.; Krom, M. D.; Bonneville, S. B. Formation of iron nanoparticles and increase in iron reactivity in mineral dust during simulated cloud processing. *Environ. Sci. Technol.* **2009**, *43*, 6592−6596.

(15) Spokes, L. J.; Jickells, T. D.; Lim, B. Solubilization of aerosol trace-metals by cloud processing − A laboratory study. *Geochim. Cosmochim. Acta* **1994**, *58*, 3281−3287.

(16) Wang, Z.; Chen, X.; Ji, H.; Ma, W.; Chen, C.; Zhao, J. Photochemical cycling of iron mediated by dicarboxylates: Special effect of malonate. *Environ. Sci. Technol.* **2010**, *44*, 263−268.

(17) Kim, K.; Choi, W.; Hoffmann, M. R.; Yoon, H.-I.; Park, B.-K. Photoreductive dissolution of iron oxides trapped in ice and its environmental implications. *Environ. Sci. Technol.* **2010**, *44*, 4142−4148.

(18) Chuang, P. Y.; Duvall, R. M.; Shafer, M. M.; Schauer, J. J. The origin of water soluble particulate iron in the Asian atmospheric outflow. *Geophys. Res. Lett.* **2005**, *32*, L07813 DOI: 10.1029/2004GL021946.

(19) Guieu, C.; Bonnet, S.; Wagener, T.; Loye-Pilot, M. D. Biomass burning as a source of dissolved iron to the open ocean? *Geophys. Res. Lett.* **2005**, *22*, L19608 DOI: 10.1029/2005GL022962.

(20) Sholkovitz, E. R.; Sedwick, P. N.; Church, T. M. Influence of anthropogenic combustion emissions on the deposition of soluble aerosol iron to the ocean: Empirical estimates for island sites in the North Atlantic. *Geochim. Cosmochim. Acta* **2009**, *73*, 3981−4003.

(21) Luo, C.; Mahowald, N.; Bond, T.; Chuang, P. Y.; Artaxo, P.; Siefer, R.; Chen, Y.; Schauer, J. Combustion iron distribution and deposition. *Global Biogeochem. Cycles* **2008**, *22*, GB1012 DOI: 10.1029/2007GB002964.

(22) Kumar, A; Sarin, M. M.; Srinivas, B. Aerosol iron solubility over Bay of Bengal: Role of anthropogenic sources and chemical processing. *Mar. Chem.* **2010**, *421*, 167−175.

(23) Schroth, A. W.; Crusius, J.; Sholkovitz, E. R.; Bostick, B. C. Iron solubility driven by speciation in dust sources to the ocean. *Nat. Geosci.* **2009**, 337−340.
(24) Seguret, M. J. M.; Kocak, M.; Theodosi, C.; Ussher, S. J.; Worsfold, P. J.; Herut, B.; Mihalopoulos, N.; Kubilay, N.; Nimmo, M. Iron solubility in crustal and anthropogenic aerosols: The Eastern Mediterranean as a case study. *Mar. Chem.* **2011**, *126*, 229−238.
(25) Srinivas, B.; Sarin, M.; Kumar, A. Impact of anthropogenic sources on aerosol iron solubility over the Bay of Bengal and the Arabian Sea. *Biogeochemistry* **2011**, DOI: 10.1007/s10533-011-9680-1.
(26) Desboeufs, K. V.; Sofikits, A.; Losno, R.; Colin, J. L.; Ausset, P. Dissolution and solubility of trace metals from natural and anthropogenic aerosol particulate matter. *Chemosphere* **2005**, *58*, 195−203.
(27) Chen, H.; Laskin, A.; Baltrusaitis, J.; Gorski, C. A.; Scherer, M. M.; Grassian, V. H. Coal fly ash as a source of iron in atmospheric dust. *Environ. Sci. Technol.* **2012**, *46*, 2112−2120.
(28) Oakes, M.; Weber, R. J.; Lai, B.; Russell, A.; Ingall, E. D. Characterization of iron speciation in urban and rural single particles using XANES spectroscopy and micro X-ray fluorescence measurements: Investigating the relationship between speciation and fractional iron solubility. *Atmos. Chem. Phys.* **2012**, *12*, 745−756.
(29) Oakes, M.; Ingall, E. D.; Lai, B.; Shafer, M. M.; Hays, M. D.; Liu, Z. G.; Russell, A. G.; Weber, R. J. Iron solubility related to particle sulphur content in source emission and ambient fine particles. *Environ. Sci. Technol.* **2012**, *46*, 6637−6644.
(30) Oakes, M.; Rastogi, N.; Majestic, B. J.; Shafer, M.; Schauer, J. J.; Edgerton, E. S.; Weber, R. J. Characterization of soluble iron in urban aerosols using near-real time data. *J. Geophys. Res.* **2010**, *115*, D15302 DOI: 10.1029/2009JD012532.
(31) Journet, E.; Desboeufs, K. V.; Caquineau, S.; Colin, J.-L. Mineralogy as a critical factor of dust iron solubility. *Geophys. Res. Lett.* **2008**, *35*, L07805 DOI: 10.1029/2007GL031589.
(32) Shi, Z.; Krom, M. D.; Bonneville, S.; Baker, A. R.; Bristow, C.; Drake, N.; Mann, G.; Carslaw, K.; McQuaid, J. B.; Jickells, T.; Benning, L. G. Influence of chemical weathering and aging of iron oxides on the potential iron solubility of Saharan dust during simulated atmospheric processing. *Global Biogeochem. Cycles* **2011**, *25*, GB2010 DOI: 10.1029/2010GB003837.
(33) Takahashi, Y.; Higashi, M.; Furukawa, T.; Mitsunobu, S. Change of iron species and iron solubility in Asian dust during the long-range transport from western China to Japan. *Atmos. Chem. Phys.* **2011**, *11*, 11237−11252.
(34) Trapp, J. M.; Millero, F. J.; Prospero, J. M. Trends in the solubility of iron in dust-dominated aerosols in the equatorial Atlantic trade winds: Importance of iron speciation and sources. *Geochem. Geophys. Geosyst.* **2010**, *11*, Q03014 DOI: 10.1029/2009GC002651.
(35) Cieré, R.; Blackford, M.; Smith, K. TEM study of $PM_{2.5}$ emitted from coal and tire combustion in a thermal power station. *Environ. Sci. Technol.* **2006**, *40*, 6235−6240.
(36) Hays, M. D.; Beck, L.; Barfield, P.; Lavrich, R. J.; Dong, Y.; Wal, R. L. V. Physical and chemical characterization of residential oil boiler emissions. *Environ. Sci. Technol.* **2008**, *42*, 2496−2502.
(37) Takahama, S.; Gilardoni, S.; Russell, L. M. Single-particle oxidation state and morphology of atmospheric iron aerosols. *J. Geophys. Res.* **2008**, *113*, D22202 DOI: 10.1029/2008JD009810.
(38) Hoffmann, P.; Dedik, A. N.; Ensling, J.; Weinbruch, S.; Weber, S.; Sinner, T.; Gutlich, P.; Ortner, H. M. Speciation of iron atmospheric aerosol samples. *J. Aerosol Sci.* **1996**, *27*, 325−337.
(39) Tong, Y; Li, A.; Cai, Y.; Ni, X.; Zhang, Y.; Wang, J.; Guo, P.; Li, X.; Zhang, G. Mössbauer study of atmospheric aerosols of Shanghai. *Environ. Sci. Technol.* **2001**, *35*, 1432−1436.
(40) Eyre, J. K.; Dickson, D. P. E. Mössbauer spectroscopy analysis of iron-containing minerals in the Chinese loess. *J. Geophys. Res.* **1995**, *100*, 17925−17930.
(41) Kopcewicz, B.; Kopcewicz, M. Mössbauer study of iron-containing atmospheric aerosols. *Struct. Chem.* **1991**, *2*, 303−312.
(42) Muxworthy, A. R.; Schmidbauer, E.; Petersen, N. Magnetic properties and Mössbauer spectra of urban atmospheric particulate matter: a case study from Munich, Germany. *Geophys. J. Int.* **2002**, *150*, 558−570.
(43) Weaver, C. E.; Wampler, J. M.; Pecuil, T. E. Mössbauer analysis of iron in clay minerals. *Science* **1967**, *156*, 3774−3776.
(44) Veranth, J. M.; Smith, K. R.; Huggins, F.; Hu, A. A.; Lighty, J. S.; Aust, A. E. Mössbauer spectroscopy indicates that iron in an aluminosilicate glass phase is the source of the bioavailable iron from coal fly ash. *Chem. Res. Toxicol.* **2000**, *13*, 161−164.
(45) Zhao, Y.; Zhang, J.; Sun, J.; Bai, X.; Zheng, C. Mineralogy, chemical composition, and microstructure of ferrospheres in fly ashes from coal combustion. *Energy Fuels* **2006**, *20*, 1490−1497.
(46) Chen, Y.; Shah, N.; Huggins, F. E.; Huffman, G. P. Investigation of the microcharacteristics of $PM_{2.5}$ in residual oil fly ash by analytical transmission electron microscopy. *Environ. Sci. Technol.* **2004**, *38*, 6553−6560.
(47) Chen, Y.; Shah, N.; Huggins, F. E.; Huffman, G. P. Transmission electron microscopy investigation of ultrafine coal fly ash particles. *Environ. Sci. Technol.* **2005**, *39*, 1144−1151.
(48) Ault, A. P.; Peters, T. M.; Sawvel, E. J.; Casuccio, G. S.; Willis, R. D.; Norris, G. A.; Grassian, V. H. Single-particle SEM−EDX analysis of iron-containing coarse particulate matter in an urban environment: Sources and distribution of iron within Cleveland, Ohio. *Environ. Sci. Technol.* **2012**, *46*, 4331−4339.
(49) Majestic, B. J.; Schauer, J. J.; Shafer, M. M. Application of synchrotron radiation for measurement of iron red-ox speciation in atmospherically processed aerosols. *Atmos. Chem. Phys.* **2007**, *7*, 2475−2487.
(50) Rubasinghege, G.; Lentz, R. W.; Scherer, M. M.; Grassian, V. H. Simulated atmospheric processing of iron oxyhydroxide minerals at low pH: Roles of particle size and acid anion in iron dissolution. *Proc. Natl. Acad. Sci. U.S.A.* **2010**, *13*, 6628−6633.